A High Capacity 3D Steganography Algorithm

Min-Wen Chao, Chao-hung Lin, Cheng-Wei Yu, and Tong-Yee Lee, *Member*, *IEEE*

Abstract—In this paper, we present a very high-capacity and low-distortion 3D steganography scheme. Our steganography approach is based on a novel multilayered embedding scheme to hide secret messages in the vertices of 3D polygon models. Experimental results show that the cover model distortion is very small as the number of hiding layers ranges from 7 to 13 layers. To the best of our knowledge, this novel approach can provide much higher hiding capacity than other state-of-the-art approaches, while obeying the low distortion and security basic requirements for steganography on 3D models.

Index Terms—Information hiding, 3D steganography, multilayered embedding.

✦

1 INTRODUCTION

STEGANOGRAPHY is a technique to hide secret messages in a host media called cover media. The advantage of steganography over cryptography is that messages do not attract attention to attackers and even receivers. Steganography and cryptography are often used together to ensure security of the secret messages [33]. For example, many previous steganography approaches [27], [28], [29], [34] use the secret key (i.e., idea borrowed from cryptography) to produce better protection of the information if the stego object arouses suspicion. Therefore, these approaches can become more secure and can be potentially useful to some security-demanding applications such as military intelligence. Watermarking is another popular technique to hide messages and it is usually used for providing ownership on copyrighted multimedia material and for detecting originators of illegally made copies. Therefore, an effective watermarking method must be robust against a variety of attacks. In contrast to watermarking, steganography prefers to hide information as much as possible and requires cover media with distortion as little as possible [1], [2].

In the past, most of the effort on steganography has been concentrated on various media data types such as an image, an audio file, or even a video file. However, there is relatively little steganography work on 3D models. With the development of 3D hardware, 3D computing or visualization has become much more efficient than ever. This leads to the widespread use of 3D models in various applications such as digital archives, entertainment, Web3D, MPEG4, and game industry. Therefore, 3D models are good candidates and rich resources to serve as the innocuous-looking hosts for hiding other types of digital content.

There have been many good 3D watermarking methods proposed [4], [5], [6], [7], [8], [9], [10], [11], [12], [13], [14], [15], [16], [17], [18], [19], [20], [21], [22], [23], [24], [25]. Most of them may be easily modified for the purpose of steganography. However, the data-hiding capacity can be very low, since they are not originally designed for this purpose. In this paper, we will exploit the geometric characteristics of 3D models to provide high-capacity data hiding. Usually, there is a trade-off between capacity, invisibility, and robustness in steganography techniques [3]. Capacity and invisibility are more important than robustness in the steganography system [1], [2], [3]. Therefore, we aim at maximizing data-hiding capacity while limiting distortion of cover models in a lower bounded value. The major contributions of this paper are listed below:

- To the best of our knowledge, our novel approach can hide much higher bit rates/vertex (i.e., 21 to 39 bits) than other previous state-of-the-art methods in steganography for 3D polygon models.
- The vertex distortion of a covert model can be limited to an upper bound $I/2$, where I is the width of a partitioning interval. The capacity and distortion of our approach depends mainly on the number of partitioning intervals. We optimize the number of partitioning intervals in terms of capacity and distortion.

2 RELATED WORKS

We describe only previous information hiding efforts for 3D polygon models. As for other cover media such as documents, images, video, and audio, a brief history and surveys can be found in [1] and [26]. Information hiding encompasses a broad range of applications in which the messages are embedded into the cover media for a variety of purposes. Watermarking and steganography are two types of information hiding. A significant number of methods have been proposed for watermarking [4], [5], [6], [7], [8], [9], [10], [11], [12], [13], [14], [15], [16], [17], [18], [19], [20], [21], [22], [23], [24], [25]. The common purpose of watermarking is to provide a robust algorithm to withstand various malicious attacks for digital content protection or to locate the modification for authenticating the integrity of

- M.-W. Chao, C.-W. Yu, and T.-Y. Lee are with the Computer Graphics Group, Visual System Laboratory, Department of Computer Science and Information Engineering, National Cheng-Kung University, No. 1, Ta-Hsueh Road, Tainan 701, Taiwan, R.O.C.
  E-mail: cvivians@hotmail.com, p7694430@ccmail.ncku.edu.tw, tonylee@mail.ncku.edu.tw.
- C.-h. Lin is with the Department of Geomatics, National Cheng-Kung University, No. 1, Ta-Hsueh Road, Tainan 701, Taiwan, R.O.C.
  E-mail: linhung@mail.ncku.edu.tw.

digital content. In general, there is a strong relationship between the embedded digital watermark and the host content. In contrast, the hidden information in steganography is kept secret to the public. Therefore, watermarking techniques are generally not suitable for the covert communication. Among these watermarking techniques, [7] and [15] could have better chances of application to steganography. After some proper modifications, [15] can hide about 0.5-1.0 bit per vertex and [7] can hide 2 bits per vertex. However, the performance of these two methods, in terms of capacity, is still much less than our approach. Instead of focusing on the robustness issue as done in most digital image watermarking research, we take capacity, reliability, and security into serious consideration. The goal is to maximize capacity while ensuring that the amount of hidden information can be transmitted without errors.

3D model watermarking technology has been actively studied in the past, but only a few works have addressed information hiding for covert communication [27], [28], [29]. In [27], the authors presented a blind information hiding scheme based on a substitution procedure in the spatial domain. This scheme is derived from the well-known quantization index modulation (QIM) [30], [31]. The basic idea is to represent a triangle as a two-state, i.e., state "0" or "1," geometrical object depending on what bit value is to be hidden. They adopted a technique called the triangle strip peeling sequence (TSPS) presented in [10] and [11] to determine the data embedding order for security considerations. In [28], the authors introduced a multilevel embedding procedure extending the scheme proposed in [27] for expanding the hiding capacity. They propose three embedding levels called sliding, extending, and rotating to embed data based on slightly shifting the vertex position. This method can provide about three times the capacity of that in [27]. In [29], the authors extended their previous work [28]. In addition to a multilevel embedding procedure, they proposed a 3D model representation rearrangement procedure to hide more data (9 bits/vertex). In contrast, our novel multilayered embedding scheme can offer up to $3n_{layers}$ bits/vertex, where n_{layers} ranged from 7 to 13 in our experiments. Our approach produces much higher hiding capacity than all of the previous works.

3 OVERVIEW OF STEGANOGRAPHIC SYSTEM

Fig. 1 schematically illustrates the proposed information hiding scheme. This scheme consists of two separate procedures: the *embedding procedure* and the *extraction procedure*. Both procedures have two main steps: *spatial analysis* and *multilayered embedding/extraction*. We briefly describe the embedding procedure. In the spatial analysis step, we analyze the cover model for obtaining a vertex embedding order and three end vertices for the payload embedding. The vertex traverse approach presented in [27] and [28] is adopted to generate the vertex embedding order. The basic idea is to represent a triangle as a pivot edge and two possible exit edges. The traverse order starts with an initial triangle and the next visited triangle is determined by the bit value in a selected secret key to take security into account. The initial triangle is determined by the principal component analysis (PCA) of the cover model. Given the
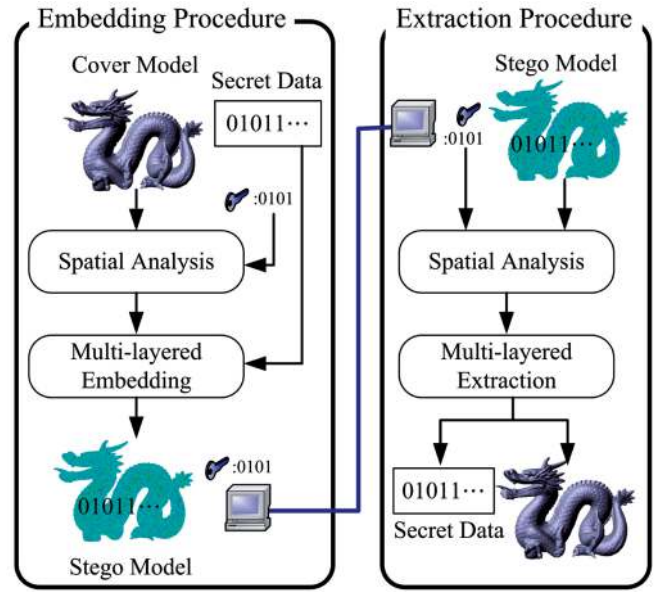

Fig. 1. System workflow.

first principal axis obtained from the PCA for the cover model, the initial triangle is the one that intersects this axis and its position is furthest from the cover model center of gravity. Once the initial triangle is determined, the next visited triangle is selected depending on the next bit value in the secret key. If the next bit value is "1," the traversal direction is the right exit edge. If the next bit value is "0," the traversal direction is the left exit edge. Once the vertex embedding order is determined, the next step is to embed the payload on the vertices in that order. In this paper, a novel multilayered embedding scheme is proposed for enlarging the hiding capacity. In the extraction procedure, the embedding order can also be obtained using the secret key in the spatial analysis step. The payload can then be correctly extracted in the reverse embedding order.

4 MULTILAYERED EMBEDDING AND EXTRACTION SCHEMES

In this section, we describe the single-layered embedding scheme first and then detail the multilayered version.

4.1 Single-Layered Embedding Scheme

First, three vertices of a cover model denoted as V_a, V_b, and V_c are selected. They are also called end vertices in this paper. These three end vertices are determined using the PCA of the cover model. Given the first and second principal axes, we orthogonally project all vertices onto these two axes. The vertices that fall on the two extreme ends of the first principal axis are selected as the end vertices V_a and V_b. The vertex that fall on the furthest extreme end of the second principal axis is selected as the third end vertex V_c. If an end vertex has multiple candidates, we simply select the nearest candidate (nearest to the principle axis) as the end vertex and slightly shift the other candidates in order to uniquely define an end vertex. The next step is to transform the cover model to align the vectors $\vec{V_a V_b}$ and $(\vec{V_a V_b} \times \vec{V_a V_c})$ with the x-axis and y-axis,
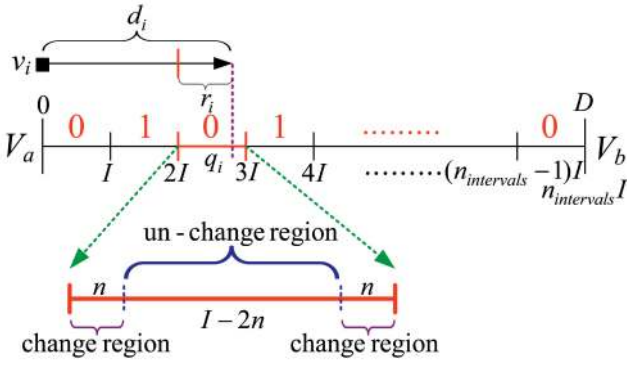
Fig. 2. An illustration of a state region q_i and its change and unchange regions. In this example, $q_i \in R_0$.

respectively, and to coincide vertex V_a with the origin of the Cartesian coordinate system. Next, we uniformly divide the line segment $\overline{V_a V_b}$ into two-state region subsets in an interleaved manner (e.g., 010101...), denoted as R_0 and R_1 in Fig. 2. The suffix of R_0 and R_1 represents the binary feature states "0" and "1," respectively. The region in which a vertex v_i falls into can be simply calculated using

$$\begin{aligned} d_i/I &= q_i \dots r_i, \\ q_i &= \lceil d_i/I \rceil, \\ r_i &= d_i \% I, \end{aligned} \qquad (1)$$

where d_i represents the projected distance between vertex v_i and the end vertex V_a on the x-axis, that is, $d_i = v_i.x - V_a.x$ (where $v_i.x$ and $V_a.x$ represent the x component of v_i and V_a, respectively). I represents the interval width of a state region, that is, $I = D/n_{intervals}$, where $n_{intervals}$ is the number of state regions and D is the distance of $\overline{V_a V_b}$. q_i then represents the state region where a vertex v_i falls into and r_i represents the vertex position in the state region q_i, as shown in Fig. 2. "%" is the remainder operator.

If $q_i \in R_0$, it implies that the bit value hidden in a vertex v_i is "0." Similarly, if $q_i \in R_1$, it implies that the bit value hidden in this vertex is "1." However, the bit value that will be embedded in a vertex depends on the hidden data and the vertex embedding order. A vertex falls in the region $q_i \in R_0$, but the hidden bit value may be "1." To solve this problem, we further divide each state region q_i into two subregions, called the *change region* and the *unchange region*, as shown in Fig. 2. The purpose of the state region subdivision is to find an empty region, i.e., the change region (no vertex falls in), over all state regions in order to proportionally move the mismatched vertices ($q_i \in R_k$ but the hidden bit value is not equal to k, where $k = 0$ or 1) to the empty region. In this manner, we not only can hide the correct bit value in each vertex but have the ability to reverse the vertex position when the hidden bit value is extracted. These two subregions can be determined using a variable n that is the minimum distance between all variables r_i and its nearest state region boundary, that is, $n = \min_i(\min(r_i, I - r_i))$, for all vertices v_i. We consider the following two cases:

Case 1. $q_i \in R_k$ and $bit(i) = k$, $k = 0$ or 1: No modification.

Case 2. $q_i \in R_k$ and $bit(i) \neq k$, $k = 0$ or 1: Shift vertex v_i to the neighboring change region in q_i, i.e., if $d_i \% I \leq I/2$,
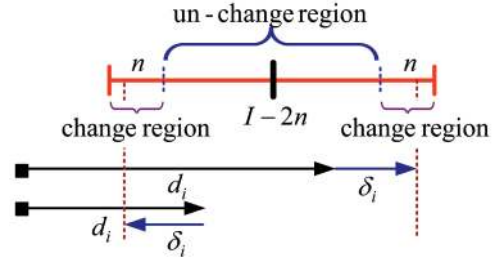

Fig. 3. Move the vertex to the neighboring change region when **Case 2** occurs.

move v_i to the change region $[0, n]$; otherwise, move v_i to the change region $[I - n, I]$, as shown in Fig. 3.

In the cases above, $bit(i)$ represents the bit value of payload hidden in a vertex v_i. In **Case 2**, the new position is calculated by adding a small offset δ_i to d_i (as shown in Fig. 3), that is,

$$d'_i = \begin{cases} d_i - \delta_i, & \text{if } r_i \leq I/2, \\ d_i + \delta_i, & \text{if } r_i > I/2, \end{cases} \qquad (2)$$

where $\delta_i = \min(r_i, I - r_i)(1 - 2n/I)$.

The drawback of the above hiding method is that n, i.e., the change region, might be too small to precisely hide a payload. We propose two approaches to solve this problem. The first approach is to optimize the number of state regions $n_{intervals}$ (Section 4.6). The goal of this optimization is to enlarge the change regions while reducing the distortion. Another approach is to enlarge the change regions by simply shrinking the unchange region to the range $[I/4, 3I/4]$ and setting the change regions to be the regions $[0, I/4]$ and $[3I/4, I]$, as shown in Fig. 4. In this manner, the small offset δ_i in (2) must be redefined as

$$\delta_i = \min(r_i, I - r_i)/2. \qquad (3)$$

Therefore, in Fig. 4, when embedding 1 bit $bit(i)$ to the vertex v_i, the new position d'_i of this vertex can be calculated using

$$d'_i = \begin{cases} d_i + (I/4 - r_i/2), & \text{if } q_i \in R_k, \ bit(i) = k, \\ d_i - \text{sgn}(I/2 - r_i)\delta_i, & \text{if } q_i \in R_k, \ bit(i) \neq k, \end{cases} \qquad (4)$$

where $\text{sgn } x = \begin{cases} -1, & \text{if } x < 0, \\ 1, & \text{if } x \geq 0. \end{cases}$

In general, the offset $|d - d'|$ must be small enough to avoid visual degradation of the cover model but large enough to allow accurate payload detection. This will be discussed in detail in Sections 4.4-4.6.
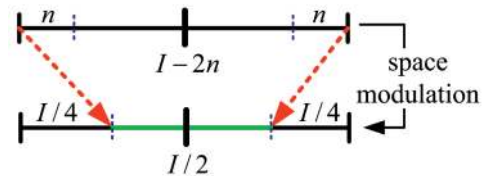

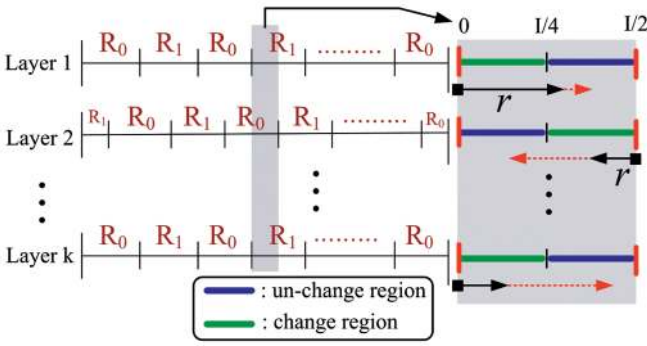Fig. 4. Modulate the spaces of change and unchange regions.

Fig. 5. An illustration of the multilayered embedding scheme. On the right side, we take a close look at the shaded interval of a state region.

4.2 Multilayered Embedding Scheme

It is very easy to extend the single-layered embedding scheme to the multilayered version by directly adding more layers, as follows: Like the single-layered version, two-state region subsets are arranged in an interleaved manner for each layer in our multilayered embedding scheme. However, we make a slight modification: the state regions in the even layers are shifted to the right by $I/2$, as shown in Fig. 5. Using this arrangement, the moving direction of a vertex is bidirectional. Vertices are swung forward and backward in the half interval of a state region when embedding payloads on them. In this manner, we can potentially hide more data on each vertex in multilayers and do not enlarge the cover model distortion. The lower bounded distortion is limited to $I/2$.

In the multilayered embedding scheme, the variable r_i for vertex v_i in (1) must be rewritten as

$$r_i = \begin{cases} d_i\%I, & \text{if embed in odd layers,} \\ (d_i + I/2)\%I, & \text{if embed in even layers.} \end{cases} \quad (5)$$

The overall multilayered embedding algorithm is processed as follows:

1. Calculate the variable d_i for each vertex v_i.
2. Calculate the variable r_i for v_i using (5).
3. Embed a payload into v_i by slightly shifting its position, i.e., variable $d_i \rightarrow d_i'$, using (4) (i.e., so v_i is shifted to a new position).
4. Repeat steps 2 and 3 for the next layer embedding until all payloads are embedded entirely on vertices.

In this manner, we can embed data on x-, y-, z-components of a vertex coordinate, respectively. In each layer, every vertex can hide 3 bits of information, except for

the end vertices V_a, V_b, and V_c. These three vertices cannot be embedded with any messages because they are the bases for the extraction process. As a result, the theoretical upper bounded capacity of our hiding scheme is $3(|V| - 3)n_{layers}$, where n_{layers} represents the number of embedding layers and $|V|$ represents the number of vertices. Each vertex swings in a $I/2$ interval using the proposed multilayered architecture. Therefore, the maximal distortion is limited to $I/2$. In Fig. 6, we show an example of our multilayered information hiding. The hiding layers number up to 10. The distortion is still imperceptible.

Note that the end vertices and initial triangle (mentioned in Section 3), obtained from cover and stego models, respectively, might not be identical if the distortion of the stego model is too large. Fortunately, this case had been very rare since the offset of vertex position is extremely small. In our experiments, the PSNR rates are all above 81 dB (shown in Tables 1 and 2). To test for robustness against this problem, we recheck if the end vertices and initial triangle are identical after data embedding.

4.3 Multilayered Extraction Scheme

In the multilayered extraction processes, the payloads are extracted in a reverse embedding order, i.e., from the last layer to the first layer, that is, extracting the bit values in reverse vertex embedding order. First, the variables d_i, q_i, and r_i for each vertex v_i can be calculated using (1) and (5). We then detect in which region (change or unchange region) the vertex lies using the following decision equation:

$$\begin{cases} v_i \in \text{change region}, & \text{if } r_i < I/4 \text{ or } r_i > 3I/4, \\ v_i \in \text{unchange region}, & \text{if } r_i \geq I/4 \text{ or } r_i \leq 3I/4. \end{cases} \quad (6)$$

The bit value $bit(i)$ embedded on the vertex v_i can be extracted by checking its state region:

$$bit(i) = \begin{cases} q_i\%2, & \text{if } v_i \in \text{unchange region}, \\ 1 - q_i\%2, & \text{if } v_i \in \text{change region}. \end{cases} \quad (7)$$

To recover the vertex position in the previous layer, we subtract the small offset δ_i back from the variable d_i [refer to (4)] and then expand the state region from $[I/4, 3I/4]$ to $[0, I]$, as shown in Fig. 7. The vertex position in the previous layer can then be calculated using the following equation, i.e., proportionally moving back to the previous layer:
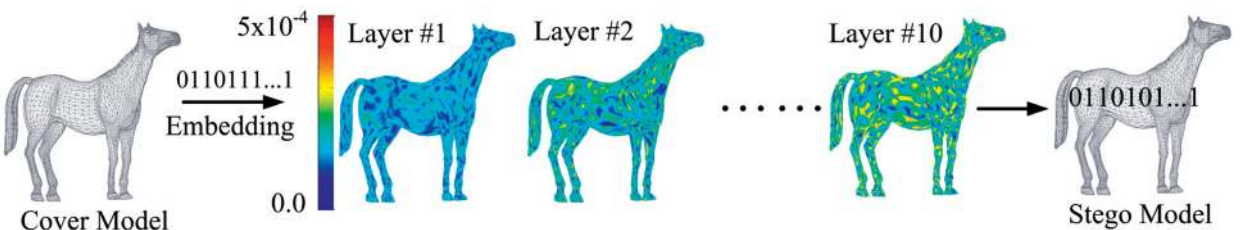

Fig. 6. An illustration of the multilayered information hiding. The hiding layers number up to 10. The distortion (measured by root-mean-square error) is coded by color ranging from blue (the smallest distortion: 0.0) to red (the largest distortion: 5×10^{-4}).

TABLE 1
Embedding Results of Various 3D Models

3D Cover models	#Vertices	n_{layers}	$n_{intervals}$	Embedded data (bit)	PSNR_1	PSNR_2
Bunny	34834	9	23500	940464	100.57	108.68
Dragon	437645	10	11785	1312920	92.75	99.71
Elephant	42321	10	13111	1269570	93.56	117.73
Skeleton-hand	1058	13	1552	41184	82.56	104.71
Horse	8431	10	8385	252870	96.16	96.75
Rabbit	67038	7	70698	1407756	107.19	122.10
Runner	7502	10	8398	225000	88.80	97.01
Teeth	116604	10	9153	3498060	91.30	110.50
Venus	134345	11	6412	4433319	89.35	111.99

The number of intervals $n_{intervals}$ is computed by (10). PSNR_1 and PSNR_2 represent the PSNR rates for position and normal distortions, respectively.

TABLE 2
The Embedding Results

Cover models	#Vertices	n_{layers}	$n_{intervals}$	Embedded data (bit)	PSNR_1	PSNR_2
Fig.15(a)	5618	8	9850	134784	98.23	124.32
Fig.15(b)	32988	9	15395	890595	101.69	107.52
Fig.15(c)	6766	8	15393	162336	101.75	81.31

$$d_i' = \begin{cases} d_i - (I/2 - r_i), & \text{if } d_i \in \text{unchange region,} \\ d_i + \mathrm{sgn}(I/2 - r_i)r_i, & \text{if } d_i \in \text{change region,} \end{cases} \quad (8)$$

where $r_i = min(r_i, I - r_i)$ and sgn is a sign function as defined in (4).

The overall multilayered extraction algorithm is processed as follows:

1. Calculate the variable d_i for each vertex v_i.
2. Calculate the variable r_i for each vertex using (5).
3. Extract a bit value from v_i using (7).
4. Recover the vertex position on the previous layer using (8).
5. Repeat steps 1-4 for the previous layer extraction until all payloads are completely extracted.

4.4 Hiding Capacity Analysis

In our experiment, the vertex coordinate is represented by IEEE 754 single precision standard format, which occupies 32 bits and has a significant precision of 23 bits (about seven decimal digits). The proposed approach hides data in the spatial domain. Therefore, the scale of 3D model will affect the hiding capacity. To faithfully measure the hiding capacity of the proposed approach, the vertex coordinates of all the experimental models are normalized to the range of 0.0 to 1.0 before data is embedded.

In our multilayer data hiding scheme, the boundaries of change and unchange subregions in a state region are at $I/4$ and $3I/4$ in the first layer. These two boundaries are shifted
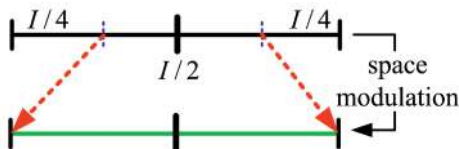

Fig. 7. State region expanding.

to $3I/8$ and $5I/8$ in the second layer due to space modulation, i.e., enlargement of the change region. Induct this to the nth layer, and these two boundaries will lie at $(2^n - 1)I/2^{n+1}$ and $(2^n + 1)I/2^{n+1}$. It means that the distance of any two adjacent boundaries in the nth embedding layer is $I/2^n$. The smallest unit (precision) of a single floating point is 2^{-23}. If the distance between these two boundaries is shorter than 2^{-23}, we cannot hide any bit in this area. Therefore, $I/2^n$ must be greater than or equal to 2^{-23}, and the limitation of the number of layers can be formulated as

$$n_{layers} \leq \log_2 I + 23. \quad (9)$$

From (9), we can see that the theoretically maximum number of hiding layers (limit) is 23 in the proposed multilayered embedding scheme. It occurs when the interval width of state region I is set to 1. It means that the number of state regions is only one, since the model is normalized to the range [0.0, 1.0] [refer to (1)]. Therefore, the theoretical hiding capacity is 69 bits/vertex (each vertex can hide 3 bits in every layer).

4.5 Floating Point Rounding Scheme

In general, we cannot hide payload up to the theoretically maximum layers due to the precision rounding error. In the IEEE 754, if a number cannot be represented in the floating point format, then the float conversion requires a choice of which float-point number is appropriate. In the IEEE 754, the default method is the round-to-even approach, which is also sometimes called banker rounding. This approach chooses the nearest value. In our embedding scheme, this rounding scheme will cause wrong bit due to the shift of the vertex to the adjacent region (wrong region). This occurs when the vertex is very close to the region boundary. Take Fig. 8 as an example. The d_i' for vertex v_i lies in the region R_b after payload embedding. The value d_i' cannot be represented in the floating point format. Therefore, it is rounded
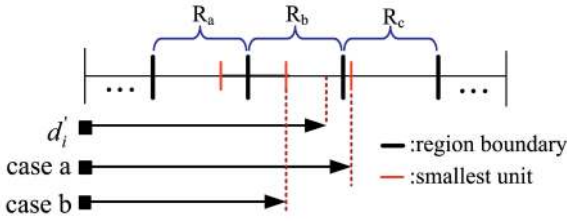
Fig. 8. Floating point rounding. Case a: Rounded to the nearest value. Case b: Rounded to the nearest value within the same region. (The red lines represent the smallest unit in standard single precision format; the black lines represent the region boundary.)

to the nearest value (case a). However, this rounding process shifts d'_i from region R_b to region R_c. This will cause wrong payload embedding. To solve this problem, we slightly modify the rounding scheme by rounding d'_i to the nearest value within the same region (as shown in case b). In this manner, we can ensure that the vertex falls in the correct region.

4.6 Interval Number Optimization

The capacity, i.e., the number of layers, and distortion mainly depend on the number of partitioning intervals in the proposed approach. A small partitioning interval can obtain a small distortion result but might hide less data, i.e., the change region is small. To balance the capacity and distortion, we find the optimal number of partitioning intervals by minimizing an objective function:

$$F(n_{intervals}) = \alpha \times Distortion + (1 - \alpha) \times Capacity, \quad (10)$$

where the instance $n_{intervals}$ represents the number of partitioning intervals, and α is a user-defined weight coefficient. In our experiments, the parameter α is set to 0.5. Both *Distortion* and *Capacity* terms are explained in the following.

The *Distortion* term is simply formulated as the root-mean-square error (RMSE). The error is defined as the distance between the vertex v_i in the cover model and its corresponding vertex v'_i in the stego model. It can also be calculated as the projected distances on the x-, y-, z-components of the vertex coordinate, that is, $(d_{ij} - d'_{ij})$, where $1 \leq j \leq 3$. The worst case of a vertex distortion occurs when a vertex is shifted to the boundaries or the center of a state region. Therefore, we formulate this term as

$$
\begin{aligned}
Distortion &= \frac{1}{|V|} \sum_{i=1}^{|V|} \sqrt{(v_i - v'_i)^2} \\
&= \frac{1}{3|V|} \sum_{i=1}^{|V|} \sum_{j=1}^{3} \sqrt{\left(d_{ij} - d'_{ij}\right)^2} \\
&= \frac{1}{3|V|} \sum_{i=1}^{|V|} \sum_{j=1}^{3} \sqrt{\left(min\left(r_{ij}, \frac{I}{2} - r_{ij}\right)\right)^2}.
\end{aligned}
\quad (11)
$$

The *Capacity* term is estimated as the width of the unchange region. A small unchange region indicates that we can have a high probability (i.e., space) to swing vertices in the half interval of a state region. This implies that it might hide more layers. We adopt the standard deviation, denoted as σ, as the estimator of this term. The confidence
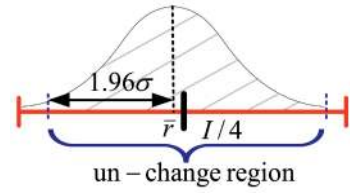

Fig. 9. Approximate the width of an unchange region in the *Capacity* term.

interval is set to be 1.96σ. It means that about 95 percent vertices have fallen in this interval for a normal distribution of vertex data. Therefore, the width of an unchange region is approximated as $2 \times 1.96\sigma$ (two sides) plus the distance between $I/4$ and the mean value of variable r, as shown in Fig. 9, that is,

$$
\begin{aligned}
\bar{r} &= \frac{1}{3|V|} \sum_{i=1}^{|V|} \sum_{j=1}^{3} r_{ij}, \\
\sigma &= \frac{1}{3|V|} \sum_{i=1}^{|V|} \sum_{j=1}^{3} \sqrt{(r_{ij} - \bar{r})^2}, \\
Capacity &= 2 \times 1.96\sigma + |I/4 - \bar{r}|.
\end{aligned}
\quad (12)
$$

Any efficient algorithm for solving the optimization problem can be adopted here. In this paper, we adopt the gradient-descent algorithm and the search range is set to $[|V|/2, 3|V|/2]$. The search space is not too large. Therefore, this process will not be time consuming. To avoid artifacts such as face fold-over in an extreme case where the interval I is larger than the half length of the smallest edge, we simply restrict its search range to be larger than $2D/|e|$, where $|e|$ represents the length of the smallest edge and the parameter D is defined previously in Section 4.1.

5   EXPERIMENTAL RESULTS

To validate the feasibility of the proposed approach, various 3D models have been selected in the experiments, as shown in Table 1 and Fig. 10. We adopt the commonly used peak signal-to-noise ratio (PSNR) to measure the distortion. Since the connectivities of the cover and stego models are identical, PSNR can be easily calculated via the RMSE of these two models. The RMSE is defined as $\sqrt{\frac{1}{|V|} \sum_i^{|V|} \|v_i - v'_i\|^2}$ and $\sqrt{\frac{1}{|V|} \sum_i^{|V|} \langle n_i, n'_i \rangle^2}$ in the position and normal distortion measurements, respectively, and PSNR is defined as $20 \log_{10}(\frac{D_{max}}{\sqrt{MSE}})$ (where D_{max} is set to the diagonal distance of the bounding box of the cover model and 180 degree in the position and normal distortion measurements, respectively).

The experimental results show that the number of layers n_{layers} ranges from 7 to 13 and the PSNR for position and normal distortions are all above 82 dB for the test models. Our approach can hide very high volumes of data, while the incurred distortion is extreme small. Note that the number of layers and the volume of embedding data shown in Table 1 are not the capacity limit of the proposed approach. As mentioned in Section 4, the layer limit is up to 23. The number of layers shown in Table 1 is the obtained optimal value for
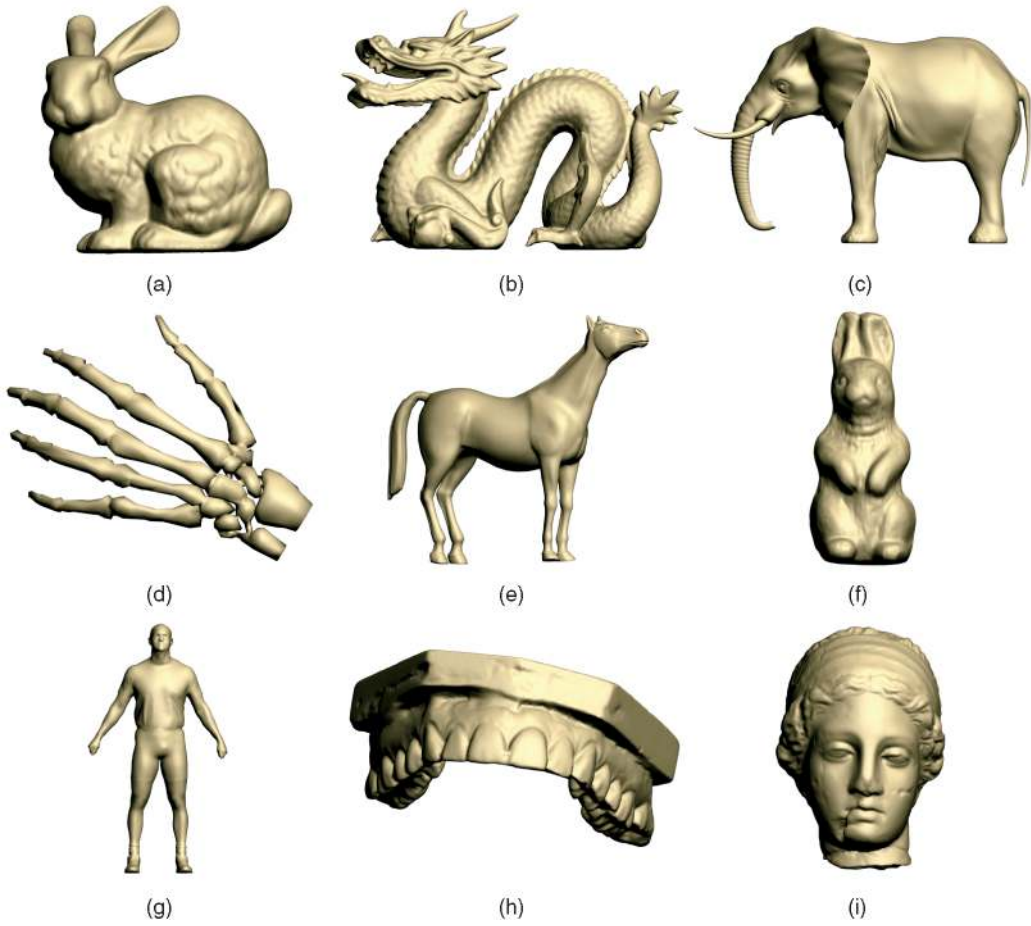
Fig. 10. Three-dimensional models in Table 1. (a) Bunny, (b) dragon, (c) elephant, (d) skeleton hand, (e) horse, (f) rabbit, (g) runner, (h) teeth, and (i) Venus.

balancing the capacity and distortion. We show the analysis of the relation between capacity (the number of layers) and distortion (PSNR) in Fig. 11. We see that PSNR rates exponentially decrease with the number of layers. The PSNR decreases sharply when the number of layers is larger than 10 (the obtained optimal value, see Table 1) in the example of a horse model. This implies that we can find a suitable $n_{intervals}$ in the optimization process. In Fig. 11, we also show the worst embedding case (the blue curve), in terms of distortion. The worst case scenario is to shift every vertex right or left by half of an interval $I/2$ in the embedding domain. Therefore, the position distortion is $20 \times \log_{10}(\frac{D_{max}}{\sqrt{I/2}})$ dB. In the case of $n_{intervals} = 8,385$, i.e., the obtained optimal partition interval number, the PSNR is still up to 87 dB. It implies that the difference between the stego and the cover models is imperceptible even for the worst embedding case. We also
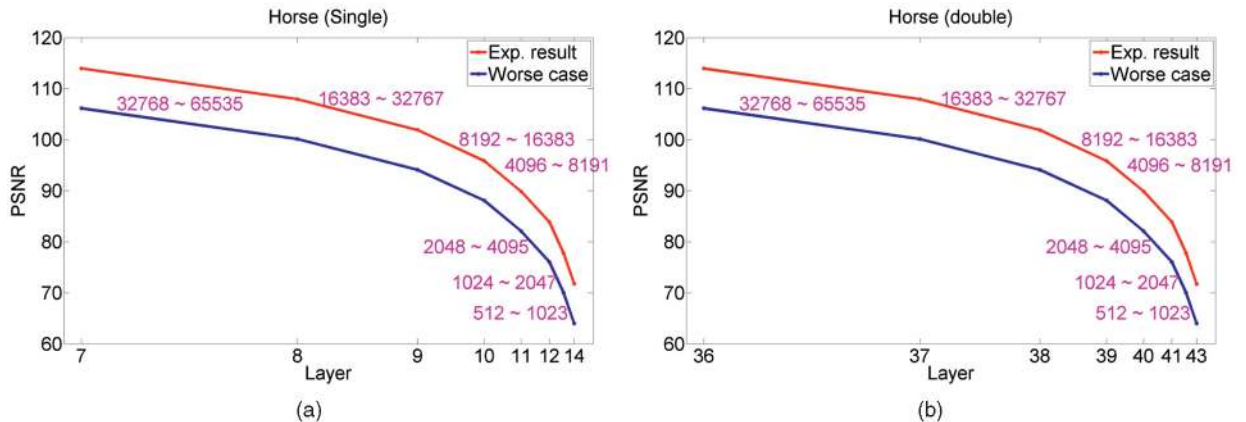

Fig. 11. The analysis of relation between the number of layers and PSNR_1 using (a) single and (b) double precision formats. The red curve is the experimental result for the horse model and blue curve is the worst case; the numbers (pink color) on the curves mean the number of intervals.
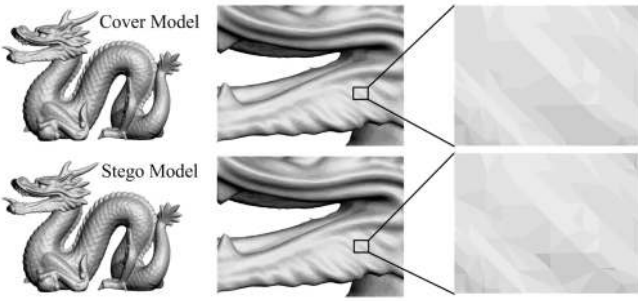
Fig. 12. Comparisons between the cover and stego models (flat shading).

Fig. 13. Comparisons between the cover and stego models (flat shading).

present the embedding analysis using the double precision standard format in Fig. 11b. The number of layers can be increased up to about 40. To further demonstrate the imperceptibility with respect to the human visual system, we synchronously magnify the local regions of the cover and stego models to perceive the detailed difference between them in Figs. 12 and 13. We also visualize the distortion encoding by colors in Fig. 14.

We experimentally evaluate our approach with two extreme cases shown in Fig. 15. Figs. 15b and 15c are generated by regularly and irregularly subdividing a local patch of Fig. 15a, respectively. Fig. 15b contains many small edges and Fig. 15c contains several near-degenerated triangles. In the experimental statistics (Table 2), both PSNR rates for vertex position and normal are high and the artifacts such as fold-over do not happen for these two extreme cases.

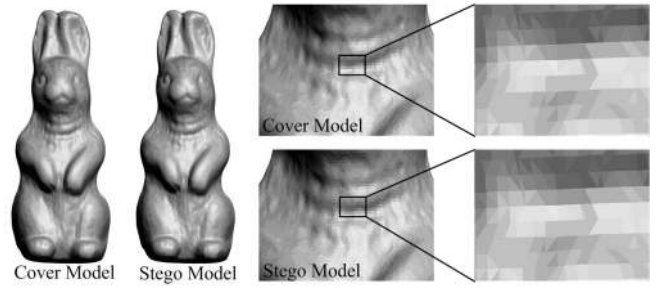Table 3 shows the theoretical comparison of the three most related steganography approaches [27], [28], [29] and

three watermarking approaches [12], [13], [16]. As expected, the steganography approaches provide more capacity but are less robust than the watermarking approaches. These four steganography approaches all belong to the blind detection schemes and hide data in the spatial domain. They can withstand similarity transformations and vertex reordering attacks (except [29]) because the vertex/face traverse orders are determined by PCA and a secret key. However, they cannot withstand attacks such as cropping, simplification, smoothing, and noise because either the vertex/face traverse orders are lost, therefore the embedded data is destroyed, or the vertices may potentially fall in incorrect regions after attacks. In other words, the embedded information cannot be recovered after suffering these malicious attacks. On the other hand, if we can find the correct vertex/face traverse orders (i.e., the receiver has the original model) after suffering the mesh simplification (assuming the simplification is done by a well-known QSlim algorithm with half-edge collapse operations [32]) or cropping attacks, we still have a chance to recover partial
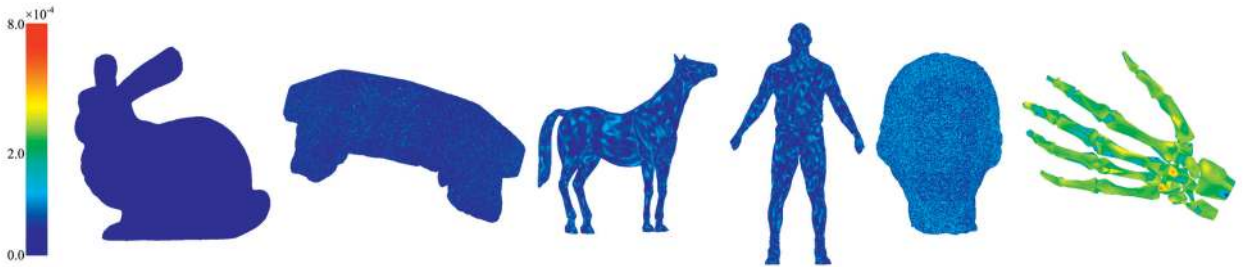

Fig. 14. The RMSE of various 3D polygon models as shown from left to right in the figure. Each model is coded by color ranging from blue (the smallest degree: 0.0) to red (the largest distortion: 8×10^{-4}).
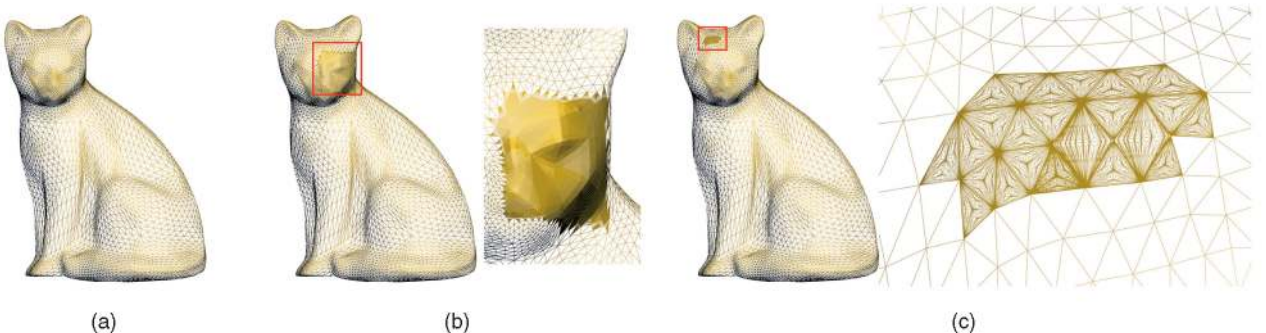

Fig. 15. The cover models: (b) and (c) are generated by regularly and irregularly subdividing a local patch of (a); (b) contains many small edges (about 85 percent of total triangles) and (c) contains several near-degenerate triangles (25 percent of total triangles).

TABLE 3
The Comparison between Our Approach and the Approaches Presented in [27], [28],
and [29] (Steganography) and [12], [13], and [16] (Watermarking)

		Steganography				Watermarking		
		[27]	[28]	[29]	Our approach	[12]	[13]	[16]
Capacity		$\sim |V|$	$3|V|$	$9|V|$	$3n_{layers}|V|$	m	m	m
Extraction scheme		blind	blind	blind	blind	non-blind	non-blind	blind
Domain		spatial	spatial	spatial	spatial	frequency	frequency	frequency
(Attacks)	Simplification	χ	χ	χ	χ	$\triangle$	$\triangle$	$\triangle$
	Cropping	χ	χ	χ	χ	$\checkmark$	$\checkmark$	χ
	Noise	χ	χ	χ	χ	$\triangle$	$\triangle$	$\triangle$
	Smoothing	χ	χ	χ	χ	$\triangle$	$\triangle$	$\triangle$
	Similarity transform	$\triangle$	$\triangle$	$\triangle$	$\triangle$	$\checkmark$	$\checkmark$	$\checkmark$
	Vertex reordering	$\triangle$	$\triangle$	χ	$\triangle$	$\checkmark$	$\checkmark$	$\checkmark$

Here, $|V|$ represents the number of vertices; m represents the size of watermark, and $|V| \gg m$; symbols "χ," "$\checkmark$," and "$\triangle$" indicate that this approach cannot withstand, can withstand, or can weakly withstand attacks, respectively.

TABLE 4
The Second and Third Columns Convey the Number of Vertices in the Cover Model (C. M.) and Attacked Model (A. M.),
Respectively; the Fourth Column Indicates the Size of the Embedded Data; the Fifth Column Relays the Extracted Data Size

Attacks	#Vertices (C.M.)	#Vertices (A.M.)	Embedded data (bit)	Extracted data (bit)	Recovery rates
Simplification (50%)	437645	218799	$1312929 \times n_{layers}$	$656334 \times n_{layers}$	50%
Simplification (75%)	437645	109251	$1312929 \times n_{layers}$	$327750 \times n_{layers}$	25%
Simplification (90%)	437645	43377	$1312929 \times n_{layers}$	$130128 \times n_{layers}$	10%
Cropping (30%)	437645	304464	$1312929 \times n_{layers}$	$913392 \times n_{layers}$	70%
Cropping (50%)	437645	218510	$1312929 \times n_{layers}$	$655530 \times n_{layers}$	50%

information. If p percent vertices are cropped or simplified, we can extract $(100 - p)$ percent of the original embedded information correctly from attacked models (see Table 4 and Fig. 16). As a result, the proposed approach and these three related steganography approaches are not suitable for the applications of digital content protection and authentication. In terms of the similarity transformation attacks, our approach is less robust than the approaches [27], [28], [29] since our approach used more mantissa of the floating point representation. Any similarity transformation, such as translation or rotation, may shift the mantissa of the floating point representation of the coordinates, thereby potentially losing some of the bit positions that are used for embedding (i.e., approximately 1 percent to 2 percent loss of the embedded information in our experiments). However, high capacity is more important than the robustness in steganography techniques. In general, embedding payload

in the spatial domain (3D space) can hide 3 bits per vertex such as the approaches presented in [28], [29], and our approach. To further increase capacity, we propose a multilayered embedding scheme that can embed data on many layers. The proposed approach offers a significant improvement in capacity compared to the previous 3D steganography methods, while the distortion is bounded.

Finally, we discuss our approach on the issue of security as follows: In all experiments, the distortion of the cover models suffered from our approach is very small, i.e., with PSNR rates > 81 dB for both vertex position and normal distortions. The visual difference between the stego and the cover models is imperceptible. Therefore, it is difficult to sense/determine whether the stego model contains any hidden messages. Our approach also allows a trade-off between the capacity and invisibility (see Fig. 11) by simply modifying the weighting coefficient α in (10). If the

Fig. 16. The first three models are simplified by 50 percent, 75 percent, and 90 percent, respectively. The last two models are cropped by 30 percent and 50 percent, respectively.

distortion factor is more important than the capacity factor, a large α can be selected. Furthermore, combining the secret key with our approach makes it harder to extract the hidden information. Therefore, we can produce better protection of the information if the stego object arouses suspicion.

6   CONCLUSIONS AND LIMITATIONS

We have introduced a novel multilayered information hiding scheme for 3D polygon models. We optimized the number of partitioning intervals to obtain a good balance between distortion and capacity. The experimental results showed that the proposed method can provide much higher capacity than previous approaches. Currently, the proposed approach has the following limitations that will be solved in the near future. Perfectly smooth (i.e., sphere) or extremely small-size models are not suitable for selection as cover models because the hidden data might be easily observed after even a very small modification by any embedding method. As in the previous work [27], [28], [29], utilizing PCA to determine the vertex traverse list may potentially hinder the robustness of the proposed method. Although the end vertices and initial triangle obtained from cover and stego models are identical in all cases in our experiments, we cannot guarantee that both are always exactly identical. One simple solution is to simply project vertices on the $x, y,$ and z-axes. However, this approach cannot withstand similarity transformations. A better approach for determining vertex traverse list is required in the near future. Another limitation is that our approach cannot withstand certain malicious attacks such as smoothing, additional noise, nonuniform scaling, simplification, and vertices resampling. As a result, the proposed approach is not suitable for the applications of digital content protection and authentication.

ACKNOWLEDGMENTS

REFERENCES

[1]   I.J. Cox, M.L. Miller, and J.A. Bloom, *Digital Watermarking.* Morgan Kaufmann, 2002.
[2]   S. Katzenbeisser and F.A.P. Petitcolas, eds., *Information Hiding Techniques for Steganography and Digital Watermarking,* Artech House, 2000.
[3]   J. Fridrich, "Applications of Data Hiding in Digital Images," *Tutorial for the ISSPA,* pp. 22-25, Aug. 1999.
[4]   O. Benedens and C. Busch, "Towards Blind Detection of Robust Watermarks in Polygonal Models," *Proc. EUROGRAPHICS '00,* pp. 199-209, Aug. 2000.
[5]   O. Benedens, "Geometry-Based Watermarking of 3-D Polygonal Models," *Proc. IEEE Computer Graphics and Applications,* special issue on image security, vol. 19, no. 1, pp. 45-46, Jan./Feb. 1999.
[6]   Y. Boon-Lock and M. Minerva, "Watermarking 3D Objects for Verification," *Proc. IEEE Computer Graphics and Applications,* special issue on image security, vol. 19, no. 1, pp. 36-45, Jan./Feb. 1999.
[7]   F. Cayre, O. Devillers, F. Schmitt, and H. Maître, "Watermarking 3D Triangle Meshes for Authentication and Integrity," INRIA Research Report RR-5223, June 2004.
[8]   F. Garcia and J. Dugelay, "Texture-Based Watermarking of 3-D Video Objects," *IEEE Trans. Circuits and Systems for Video Technology,* vol. 13, no. 8, pp. 853-866, Aug. 2003.
[9]   H.-Y. Lin, H.-Y. Liao, C.-S. Lu, and J.-C. Lin, "Fragile Watermarking for Authenticating 3D Polygonal Meshes," *IEEE Trans. Multimedia,* vol. 7, no. 6, pp. 997-1006, Dec. 2005.
[10] R. Ohbuchi, H. Mazuda, and M. Aono, "Watermarking Three-Dimensional Polygonal Models," *Proc. Fourth ACM Int'l Conf. Multimedia (ACM Multimedia '97),* pp. 261-272, 1997.
[11] R. Ohbuchi, H. Mazuda, and M. Aono, "Watermarking Three-Dimensional Polygonal Models through Geometric and Topological Modifications," *IEEE J. Selected Areas in Comm.,* vol. 16, no. 4, pp. 551-560, 1998.
[12] R. Ohbuchi, A. Mukaiyama, and S. Takahashi, "A Frequency-Domain Approach to Watermarking 3D Shapes," *Computer Graphics Forum,* vol. 21, no. 3, pp. 373-382, 2002.
[13] E. Praun, H. Hoppe, and A. Finkelstein, "Robust Mesh Watermarking," *Proc. ACM SIGGRAPH '99,* pp. 49-56, 1999.
[14] K. Yin, Z. Pan, S. Jiaoying, and D. Zhang, "Robust Mesh Watermarking Based on Multiresolution Processing," *Computers and Graphics,* vol. 25, pp. 409-420, 2001.
[15] H.-T. Wu and Y.-M. Cheung, "A Reversible Data Hiding Approach to Mesh Authentication," *Proc. IEEE/WIC/ACM Int'l Conf. Web Intelligence (WI '05),* pp. 774-777, Sept. 2005.
[16] S. Zafeiriou, T. Anastasios, and I. Pitas, "Blind Robust Watermarking Schemes for Copyright Protection of 3D Mesh Objects," *IEEE Trans. Visualization and Computer Graphics,* vol. 11, no. 5, pp. 596-607, Sept./Oct. 2005.
[17] V.R. Doncel, N. Nikolaidis, and I. Pitas, "An Optimal Detector Structure for the Fourier Descriptors Domain Watermarking of 2D Vector Graphics," *IEEE Trans. Visualization and Computer Graphics,* vol. 13, no. 5, Sept./Oct. 2007.
[18] Y.-Q. Ni, B. Liu, and H.-B. Zhang, "A Blind Watermarking of 3D Triangular Meshes Using Geometry Image," *Proc. Fourth Int'l Conf. Computer Graphics, Imaging and Visualization (CGIV '07),* pp. 335-340, 2007.
[19] O. Benedens, "Affine Invariant Watermarks for 3D Polygonal and Nurbs Based Models," *Proc. Third Int'l Workshop Information Security (ISW '00),* pp. 329-340, Dec. 2000.
[20] T. Harte and A.G. Bors, "Watermarking 3-D Models," *Proc. IEEE Int'l Conf. Image Processing (ICIP '02),* vol. III, pp. 661-664, Sept. 2002.
[21] O. Benedens, "Robust Watermarking and Affine Registration of 3D Meshes," *Proc. Fifth Int'l Workshop Information Hiding (Information Hiding '03),* pp. 177-195, 2003.
[22] H. Date, S. Kanai, and T. Kishinami, "Digital Watermarking for 3D Polygons Model Using Multiresolutional Wavelet Decomposition," *Proc. Sixth IFIP WG 5.2 Int'l Workshop Geometric Modeling: Fundamentals and Applications (GEO-6 '98),* pp. 296-307, Dec. 1998.
[23] R. Ohbuchi, S. Takahashi, T. Miyasawa, and A. Mukaiyama, "Watermarking 3-D Polygonal Meshes in the Mesh Spectral Domain," *Proc. Computer Graphics Interface,* pp. 9-17, June 2001.
[24] H. Song, N. Cho, and J. Kim, "Robust Watermarking of 3D Mesh Models," *Proc. IEEE Int'l Workshop Multimedia Signal Processing (MMSP '02),* pp. 332-335, Dec. 2002.
[25] A. Kalivas, A. Tefas, and I. Pitas, "Watermarking of 3D Models Using Principal Component Analysis," *Proc. IEEE Int'l Conf. Acoustics, Speech, and Signal Processing (ICASSP '03),* vol. 5, pp. 676-679, Apr. 2003.
[26] F.A.P. Petitcolas, R.J. Anderson, and M.G. Kuhn, "Information Hiding—A Survey," *Proc. IEEE,* special issue on protection of multimedia content, vol. 87, no. 7, pp. 1062-1078, 1999.
[27] F. Cayre and B. Macq, "Data Hiding on 3-D Triangle Meshes," *IEEE Trans. Signal Processing,* vol. 51, no. 4, pp. 939-949, 2003.
[28] C.-M. Wang and Y.-M. Cheng, "An Efficient Information Hiding Algorithm for Polygon Models," *Proc. Eurographics '05,* vol. 24, no. 3, pp. 591-600, 2005.
[29] Y.-M. Cheng and C.-M. Wang, "A High-Capacity Steganographic Approach for 3D Polygonal Meshes," *The Visual Computer,* vol. 22, no. 9, pp. 845-855, 2006.

[30] B. Chen and G.W. Wornell, "Quantization Index Modulation: A Class of Provably Good Methods for Digital Watermarking and Information Embedding," *IEEE Trans. Information Theory,* vol. 47, no. 4, pp. 1423-1443, May 2001.

[31] F. Perez-Gonzalez and F. Balado, "Quantized Projection Data Hiding," *Proc. IEEE Int'l Conf. Image Processing (ICIP '02),* vol. 2, pp. 889-892, Sept. 2002.

[32] M. Garland and P.S. Heckbert, "Surface Simplification Using Quadric Error Metrics," *Proc. ACM SIGGRAPH '97,* pp. 209-216, 1997.

[33] *The Wiki www Site,* http://en.wikipedia.org/wiki/Steganography, 2008.

[34] L. Marvel, C. Boncelet, and J. Retter, "Spread Spectrum Image Steganography," *IEEE Trans. Image Processing,* pp. 1075-1083, Aug. 1999.

Cheng-Wei Yu received the BS degree from the National Central University, Jhongli, Taiwan, in 2005 and the MS degree from the National Cheng-Kung University, Tainan, Taiwan, in 2007. He is currently with the Department of Computer Science and Information Engineering, National Cheng Kung University.

Min-Wen Chao received the BS degree in mathematics and the MS degree from the National Cheng Kung University, Tainan, Taiwan, in 2003 and 2005, respectively. She is currently working toward the PhD degree in the Department of Computer Science and Information Engineering, National Cheng-Kung University. Her research interests include computer graphics and data hiding.

Chao-hung Lin was born in Koushung, Taiwan, in 1973. He received the BS degree in computer science/engineering from Fu-Jen University and the MS and PhD degrees in computer engineering from the National Cheng-Kung University, Tainan, Taiwan, in 1997, 1998, and 2004, respectively. He is currently an assistant professor in the Department of Geomatics, National Cheng-Kung University. His current research interests include computer graphics, image processing, visualization, and modeling.

Tong-Yee Lee received the PhD degree in computer engineering from Washington State University, Pullman, in 1995. He is currently a full professor in the Department of Computer Science and Information Engineering, National Cheng-Kung University, Tainan, Taiwan. He leads the Computer Graphics Group, Visual System Laboratory, National Cheng Kung University (http://graphics.csie.ncku.edu.tw/). His current research interests include computer graphics, nonphotorealistic rendering, image-based rendering, visualization, virtual reality, surgical simulation, medical visualization and medical system, and distributed and collaborative virtual environments. He is an associate editor for the *IEEE Transactions on Information Technology in Biomedicine* from 2000 to 2010. He is also on the editorial advisory board of the journal *Recent Patents on Engineering*, an editor of the *Journal on Information Science and Engineering*, and a region editor of the *Journal of Software Engineering*. He served as a member of the international program committees of several conferences including IEEE Visualization, Pacific Graphics, the IEEE Pacific Visualization Symposium, IEEE Virtual Reality, the IEEE-EMBS International Conference on Information Technology and Applications in Biomedicine, the International Conference on Artificial Reality and Telexistence, and the International Conference in Central Europe on Computer Graphics, Visualization, and Computer Vision. He is a member of the IEEE and the ACM.

▷ **For more information on this or any other computing topic, please visit our Digital Library at** www.computer.org/publications/dlib.